Steel and Composite Structures, *Vol. 18, No. 1 (2015) 273-288*
DOI: http://dx.doi.org/10.12989/scs.2015.18.1.273

Case study on stability performance of asymmetric steel arch bridge with inclined arch ribs

Xinke Hu [1], Xu Xie [*1], Zhanzhan Tang [1a], Yonggang Shen [1], Pu Wu [2] and Lianfeng Song [2]

[1] *Department of Civil Engineering, Zhejiang University, China*
[2] *Architectural design and Research Institute of Zhejiang University, Hangzhou, Zhejiang, China*

(*Received April 28, 2012, Revised January 15, 2014, Accepted June 19, 2014*)

Abstract. As one of the most common failure types of arch bridges, stability is one of the critical aspects for the design of arch bridges. Using 3D finite element model in ABAQUS, this paper has studied the stability performance of an arch bridge with inclined arch ribs and hangers, and the analysis also took the effects of geometrical and material nonlinearity into account. The impact of local buckling and residual stress of steel plates on global stability and the applicability of fiber model in stability analysis for steel arch bridges were also investigated. The results demonstrate an excellent stability of the arch bridge because of the transverse constraint provided by transversely-inclined hangers. The distortion of cross section, local buckling and residual stress of ribs has an insignificant effect on the stability of the structure, and the accurate ultimate strength may be obtained from a fiber model analysis. This study also shows that the yielding of the arch ribs has a significant impact on the ultimate capacity of the structure, and the bearing capacity may also be approximately estimated by the initial yield strength of the arch rib.

Keywords: stability; asymmetric steel arch bridge; inclined arches; elasto–plastic large deformation; local buckling; residual stress

1. Introduction

Instability of arch ribs is a common failure type for steel arch bridges which requires a particular attention in the design. Many researchers studied the stability of steel arch ribs so far. Austin and Ross (1976) and Dadeppo and Schmidt (1969) established stability theory of bare arch ribs to calculate the elastic instability factors. Kim *et al*. (2003) developed a performance based design method to perform inelastic nonlinear analysis for three-dimensional steel arch bridges by beam structural models. Cheng (Cheng *et al.* 2003, Cheng and Li 2009) calculated the ultimate capacity of Lu Pu arch bridge under static wind loads which had significant effects on the bridge. Xie *et al*. (2004) studied the impact of load pattern to the ultimate capacity of long-span two-hinged arch bridges, and the results showed that the structure will become unstable as soon as the initial yielding on arch ribs occurs, and the capacity of the structure will be improved when the

*Corresponding author, Professor, Ph.D., E-mail: xiexu@zju.edu.cn
[a] Ph.D. Student, E-mail: tangzhanzhan@126.com

http://www.techno-press.org/?journal=scs&subpage=8 ISSN: 1229-9367 (Print), 1598-6233 (Online)

stiffening girder has higher yield strength. Romeijn and Bouras (2008) analyzed the effective length factor of arch rib for a tied arch bridge, and compared the factors with that of Eurocode 3 for validating the values adopted by the specifications. Moon *et al*. (2009) studied a flat parabolic arch and proposed amendment to the effective length factor adopted by AASHTO LRFD provisions. Wei *et al*. (2009) studied a steel parabolic arch bridge using beam element model with consideration of the elastic–plastic large deformation, and proposed the formulas to calculate the strength of the arch ribs. Some other researchers, such as Pi (2010a, b, c) and Cai *et al*. (2012), studied the influence of thermal effects and boundary conditions on the in-plane stability of circular and parabolic shallow arch ribs. Cai and Feng (2010) studied the in-plane stability of parabolic shallow arches with elastic supports and established the nonlinear buckling equilibrium equations for the scenario when the stiffness of supports increases with the axial force.

These studies improved the design methodology of arch bridges, but the results obtained from these studies were based on the beam element model, which cannot consider the effect of local buckling and plasticity due to 3D torsional deformation.

Arch bridge is a structure type with many varieties. The adoption of high strength steel cable as the hangers and ties makes the structure behaves significantly different between some varieties. Therefore it is hard to evaluate its capacity just through the in-plane or out-of-plane stability analysis. The carrying capacity of the ribs should consider not only the axial force in the rib, but also the biaxial bending moment and torsion.

This research studied the spatial stability and ultimate capacity of a real bridge with transversely-inclined arch ribs and hangers. The research accounted for the elasto–plastic large deformation and local buckling, studied the mechanism of the instability and the methodology to calculate the stability capacity. The research results may provide reference for the design of similar arch bridges.

2. Description of the bridge and FE model

2.1 Description of the bridge

The exemplary bridge used in this study is Dinghu Bridge with a span length of 90.8 m in Lishui City, China. As shown in Fig. 1, the bridge is asymmetrical with two transversely-inclined arch ribs and hangers and steel box girder, the lane layout at the center span is 5.5 m (pedestrian) + 4.75 m (hollow area) + 8 m (driveway) + 2.5 m (separation belt) + 8 m (driveway) + 4.75 m (hollow area) + and 7 m (pedestrian). The girder of the driveway takes a uniform box cross-section, the girder for pavement takes a variable width box cross-section, and the steel I-beams connect the girders in transverse direction. The bridge satisfies the stress and deformation requirements per Chinese highway bridge code under I level live load (lane load of 10.5 kN/m and concentrated load of 360 kN), and the pedestrian load is 3.5 kN/m^2. Both arches are in parabolic shape, the rise-to-span ratio is 0.3094 for the larger arch rib and 0.1944 for the smaller one, the inclination angle in transverse direction is 16° and 20° relative to vertical direction. Each rib has interior and exterior hangers in which 20 interior hangers are used as the main hangers, while 16 exterior ones as the secondary hangers. For interior hangers, they have circular cross-sectional area of 0.0017 m^2 and initial tension from 195 to 402 kN at the larger arch rib and 199 to 381 kN at the smaller one. For exterior hangers, they have circular cross-sectional area of 0.00042 m^2, and initial tension of 20 kN at the larger arch rib and 15 kN at the smaller one. The cross-section of the smaller arch rib

is uniform steel box, and that of the larger arch rib is variable steel box. The average diaphragm spacing is 2.0 m.

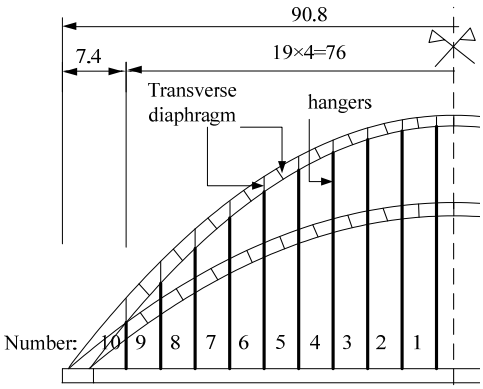

(a) Elevation

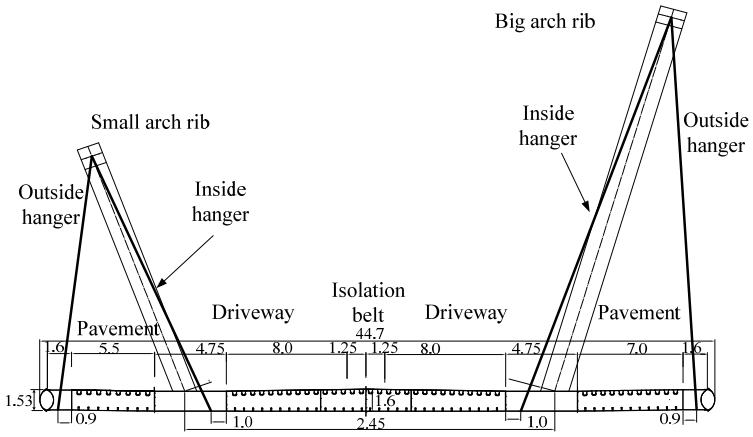

(b) Deck cross-section at the center span

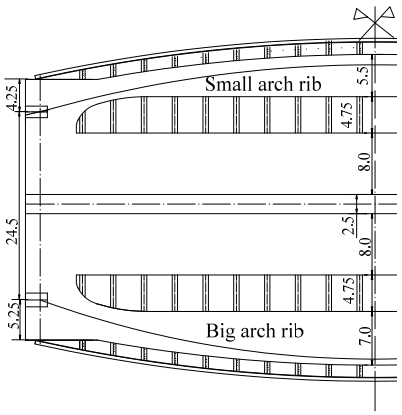

(c) Plan

Fig. 1 Details of the bridge structure (units: m)

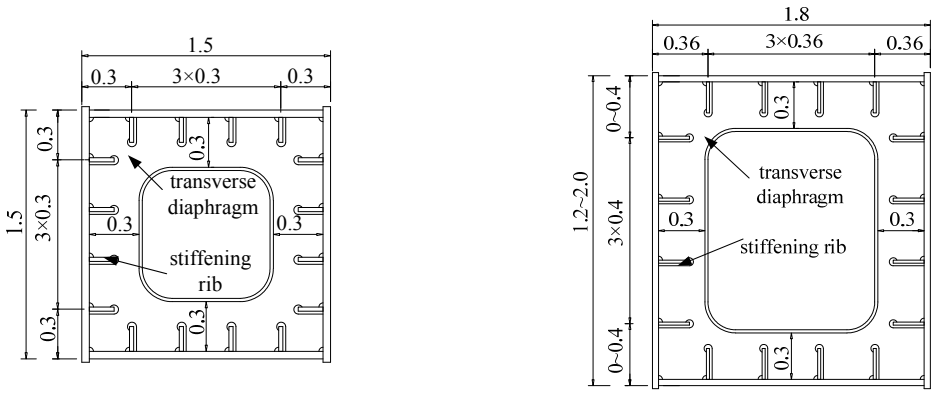

(d) Cross-sections of the arch ribs

Fig. 1 Continued

2.2 Model and material property

The FE model was built by ABAQUS 6.9 in which arch ribs and bridge deck were modeled by shell elements, and hangers were modeled by truss elements. Fig. 2 shows the full bridge model, with a total of approximate 256,000 shell elements and 72 truss elements. In order to investigate local buckling of steel plate on global stability, a fiber model whose arch rib was modeled by fiber elements was also employed.

The yield strength of arch ribs and girders is 345 MPa, the Young's modulus is 2.06×10^5 MPa, and Poisson's ratio is 0.3. The hangers are composed of high strength steel wires whose yield strength is 1650 MPa, ultimate strength is 1860 MPa, and Young's modulus is 1.95×10^5 MPa. The Young's modulus of the two materials is taken as 1% of the initial one during strength hardening stages. Fig. 3 shows the relationship of stress-strain of the materials.

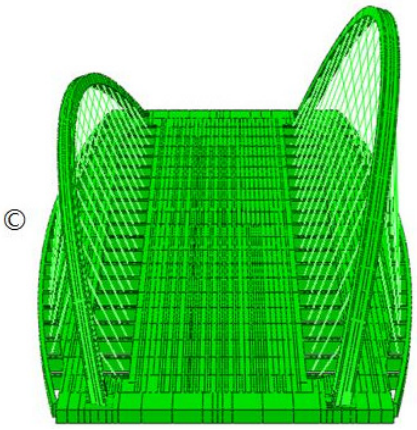

(a) Geometry of modeled bridge

Fig. 2 Full and local model of FEM

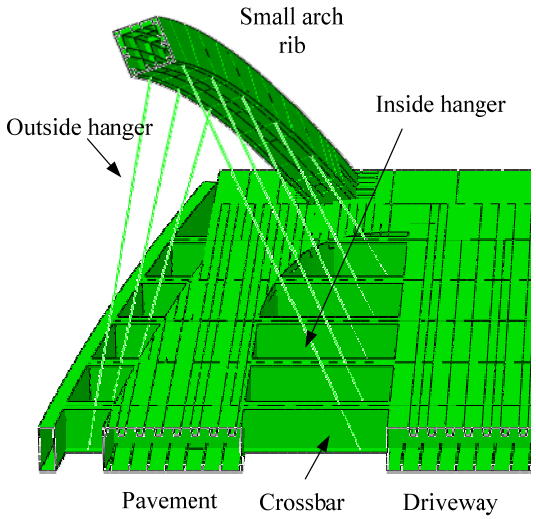

(b) Local modeled bridge

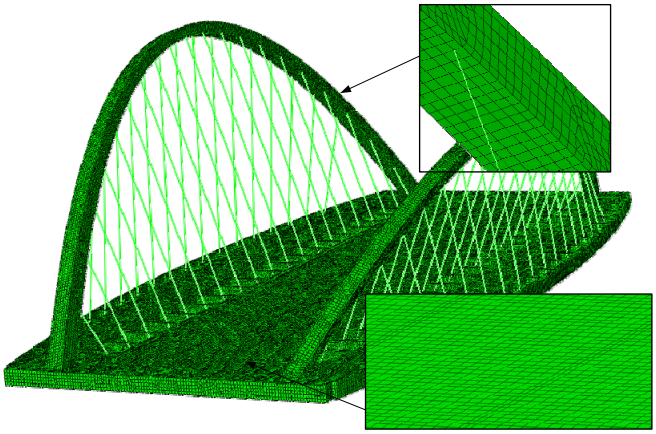

(c) Meshed model

Fig. 2 Continued

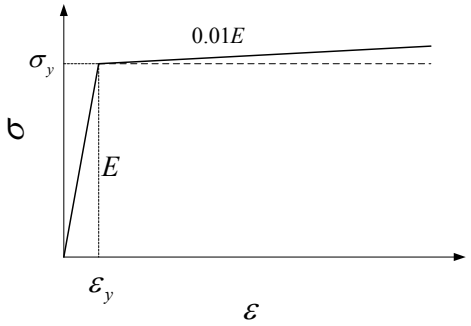

Fig. 3 Stress-strain curve of the material

2.3 Load cases

The dead load includes structural weight, superimposed dead load, and initial tension force in hangers, live load includes vehicle load (lane load plus concentrated force) and pedestrian loads. The lane loads are converted into uniformly distributed load along the entire lane width, and the concentrated loads are converted into transverse line load applied at mid-span to facilitate the calculation. Fig. 4 shows the four load cases analyzed in the study.

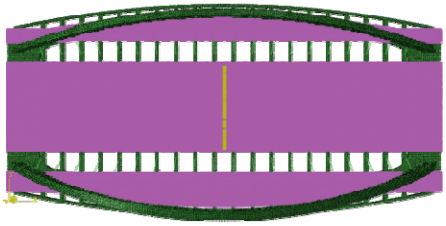

(a) Case 1：Dead load + initial hanger tension + entire live load

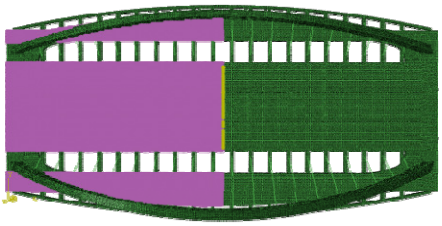

(b) Case 2：Dead load + initial hanger tension + half live load

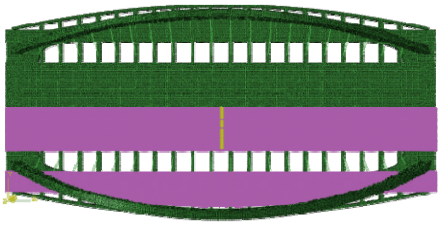

(c) Case 3：Dead load + initial hanger tension + large-arch-side live load

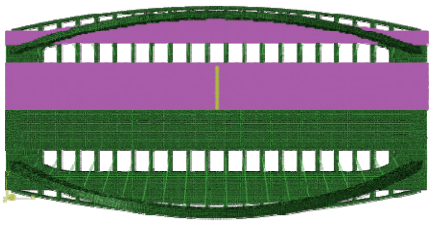

(d) Case 4：Dead load + initial hanger tension + small-arch-side live load

Fig. 4 Distribution of live load

3. Results and discussions

Arc-length method was used during the analysis, and the loads gradually increased following a certain pattern to obtain the ultimate capacity of the structure. The factor used to scale the loads, i.e., Load Proportionality Factor (LPF), considers both dead load and live load. The completed bridge state was used as the initial state to apply the loads.

3.1 Stress distribution of the completed bridge state

Fig. 5 shows the Mises stress distribution when the bridge is completed. The maximum stress is 86 MPa and located at the exterior side of the end of smaller rib, and the average stress level of the rib is 40 MPa.

3.2 The ultimate state of the structure

Fig. 6 shows the deformation of the structure at maximum LPF state relative to the undeformed structure. The ribs have dominant displacement in transverse direction, and the maximum deformation occurs at the top of the ribs. This deformation pattern is mainly caused by the arrangement of the ribs and hangers.

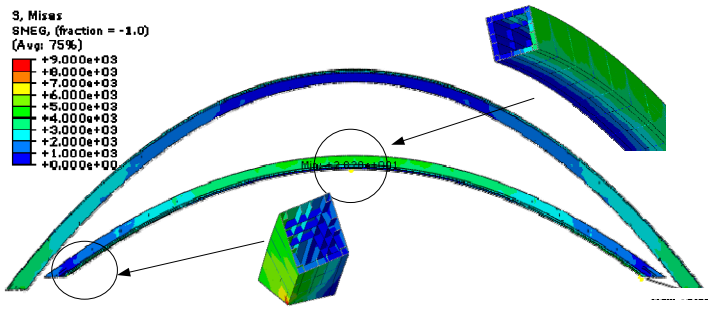

Fig. 5 Stress field when the bridge is completed (unit: 0.01 MPa)

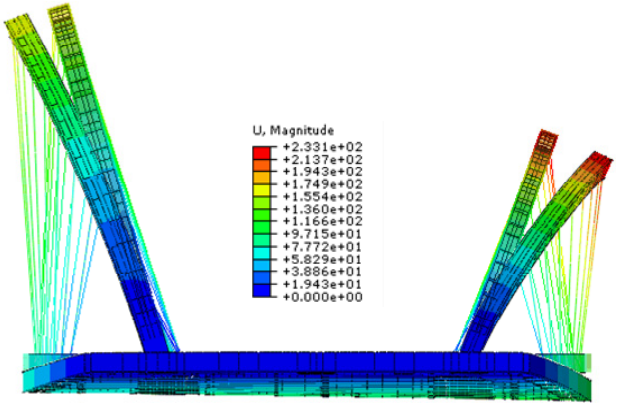

Fig. 6 Overall deformation when LPF reaches the maximum in case 1 (unit: cm)

To investigate the relationship between local buckling and the ultimate capacity, this study uses the result of the cross-section at the top of the smaller rib where the maximum deformation occurs, to analyze the deformation process of the cross-section. Fig. 7 shows the rib's lateral deformation due to load case 4, the deformation of the cross-section is not obvious before the plastic region occurs, as the load increases the deformation of the cross-section at the top of the rib is mainly point to outward in transverse direction. When the LPF reaches the maximum, the deformation is still not large enough to induce local buckling, at the ultimate capacity, the inside surface of the plate bulges outward, and the upper and lower surfaces of the plate bulges separately upward and

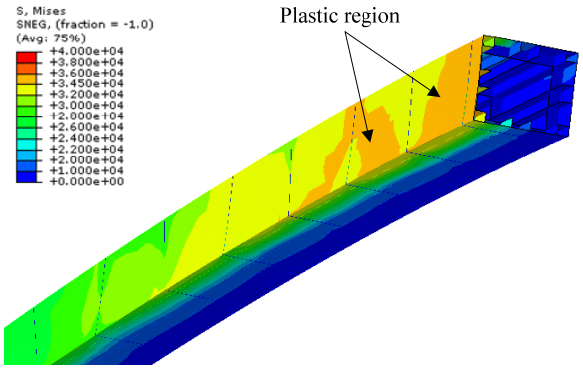

(a) When the plastic region occurs in the rib (LPF = 4.52)

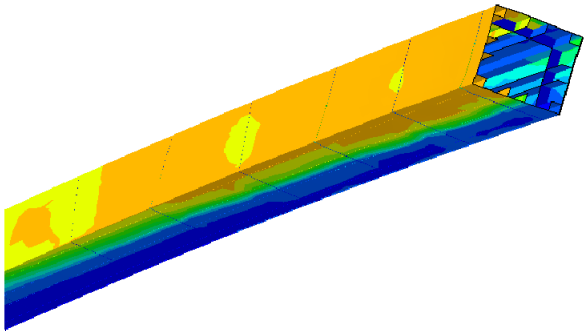

(b) When the rib reaches its maximum load (LPF = 4.81)

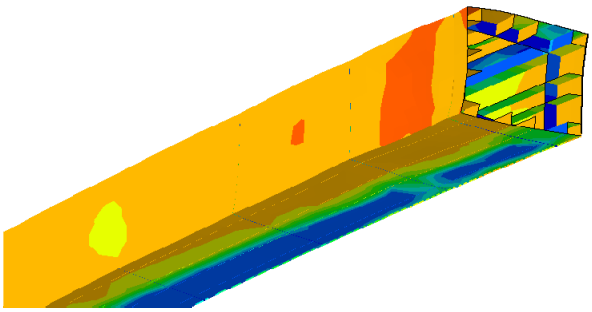

(c) After the maximum load (LPF = 4.35)

Fig. 7 Local deformation at the crown of the smaller rib under load case 4

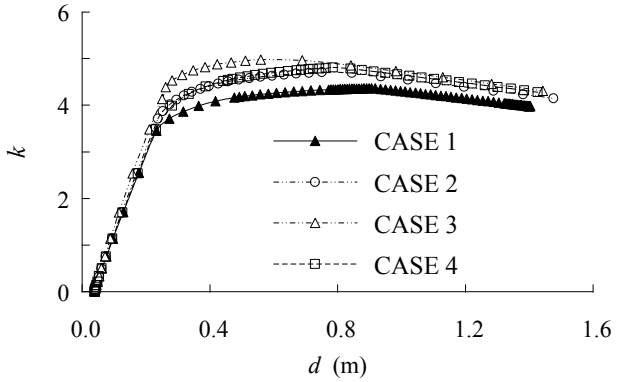

Fig. 8 Curves of the LPF *k* vs vertical displacement *d*

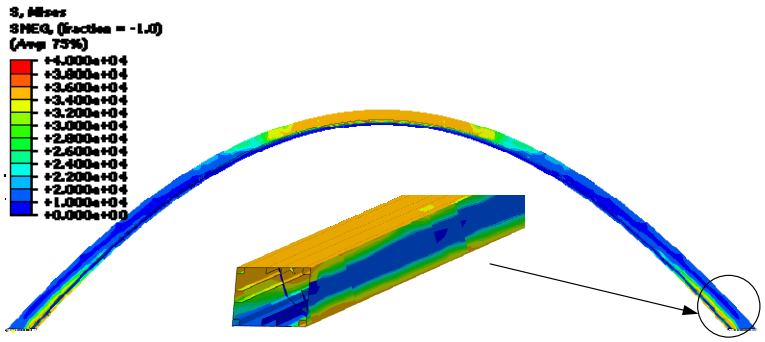

(a) Large arch rib

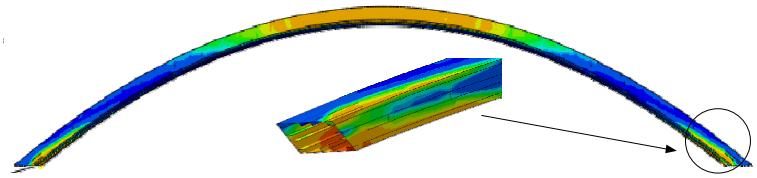

(b) Small arch rib

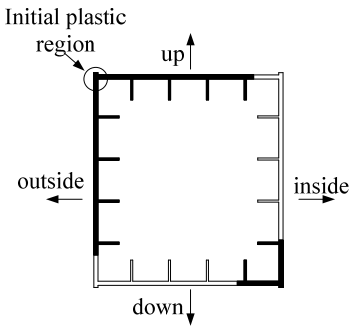

(c) Foot of the arch

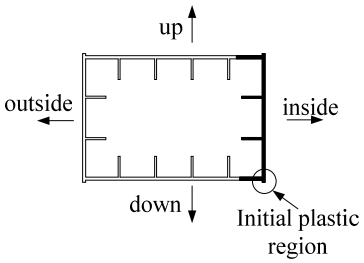

(d) Apex of the arch

Fig. 9 Distribution of the plastic region in the limited state (dark part)

downward at the location without diaphragms. Therefore, the local buckling caused by the large deformation occurs after the instability of the whole rib which means the local deformation cannot control the overall instability of the structure. Thus, another controlling factor must be found.

Fig. 8 shows the load factor (k)-vertical displacement (d) curves at the crown of the larger arch rib, and when k is 0, the structure is at the initial stage of the completed bridge state. The results show that the load-displacement curves are close to each other at the beginning under the four load cases, the discrepancy was observed after plastic region occurs. When the structure reaches the limited state, the strength has no significant decrease for the constraints of the inclined hangers to the ribs. The minimum ultimate load factor among all the load cases occurs in load case 1, which indicates that case 1 is the governing load case. Therefore, the bearing capacity of the structure will be analyzed further for this load case later in this paper.

The appearance of plastic region on the arch rib is the major cause of structure instability. Fig. 9 shows the distribution of the plastic region on the rib when the load reaches the maximum (case 1). The load type on the bridge has little effect on the distribution of the plastic region at the limited state of the structure. As shown in the figure, the plastic regions are located from the arch foot to 1/4 span of the rib and the interior side around the top of the rib. The first plastic area occurs at the exterior side of the cross section and nearby stiffeners of the foot of the small arch, and gradually develops along the arch upward, and then the plastic region appears at the exterior side at the foot of large rib and the interior side at the top of the smaller arch. The plastic region does not spread to the full cross-section, but usually appears simultaneously at the surface plate and nearby stiffeners. Fig. 9 (c and d) shows the plastic region distribution described above.

3.3 Effect of hanger on the overall stability

The bearing capacity of the arch bridge is determined by the rib and the hangers as the inclined hangers restrain the lateral deformation of the ribs. Therefore, the stiffness of the hangers significantly affects the ultimate capacity of the structure.

Fig. 10 shows the tensile stress of the interior hangers of the larger arch due to load case 1. The stress of the main hanger increases as the LPF increases. When the plastic region appears in the rib, the hangers located in the mid-span of the structure also yield. As the load continues to increase, the forces are redistributed among other hangers and cause the other hangers yield as well. Before

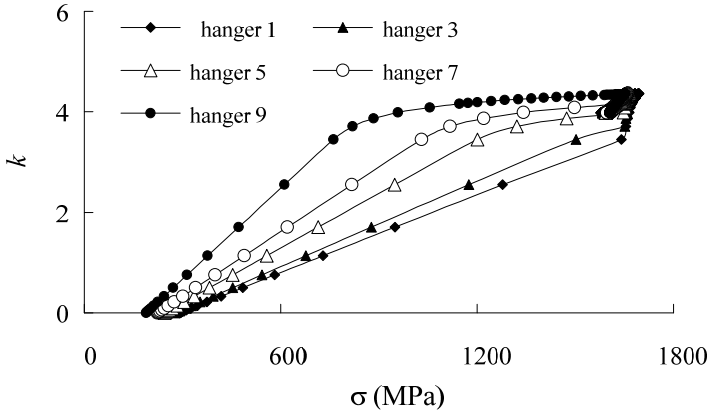

Fig. 10 Result of tensile stress in the inside hangers of large arch in case 1

Table 1 LPF of the rib

Load Case	Initial yield of hangers	Initial yield of arch rib	Last yield of hangers	Limited state
1	3.45	3.71	4.35	4.36
2	3.71	3.87	4.54	4.71
3	4.10	4.13	4.88	4.98
4	3.95	3.98	4.52	4.81

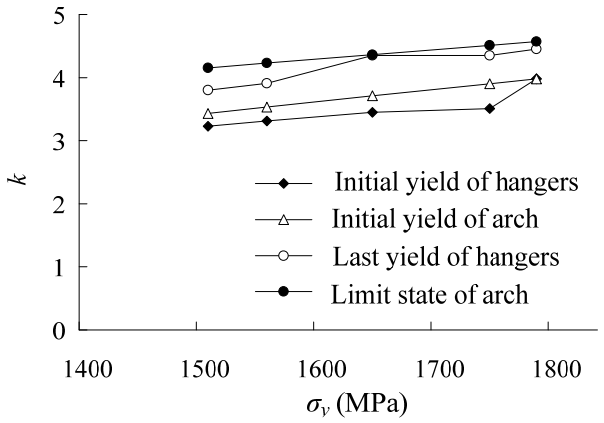

Fig. 11 Effect of the yield strength of the hanger on the ultimate strength of the structure

the structure reaches the limit state, all the interior hangers yield with the principal tensile stress of 1650 MPa, but none of them reach the ultimate strength of 1860 MPa. After reaching the ultimate load, all the interior hangers experience an unloading process.

Table 1 shows the results of the initial yield load factor of the hangers and ribs, the ultimate yield load factor of all hangers, and the limited state load factor of the structure. The initial yield stage of hangers occurs before the rib's initial yielding, suggesting that the yield of the hangers may initiate the buckling of the rib. Furthermore, the hangers that yield first are all located near the mid-span, and the first yielding location of the rib is at the arch foot. After all the interior hangers yield, the lateral constraints of the arch decreases, which may make the structure reach its ultimate capacity state quickly. When the arch rib reaches its initial yielding state, the structure can only bearing about 15% of the ultimate load more. Actually, when take initial imperfection of the arch rib into consideration, the remaining carrying capacity maybe less than 15%.

We further analyzed the influence of the hangers' strength on the structure's ultimate capacity by varying the yield strength and ultimate strength of the hangers, and the results are shown in Fig. 11. The horizontal axis is the yield strength of the hangers. The results show that when the yield strength of the hanger increases to a certain level, the initial yield load factor is equal to the first yield load factor of rib, and the limit load factor of the bridge increases. Increasing the yield strength can improve the ultimate capacity of the entire bridge because this would improve the overall stability of the rib when the arch reaches its limit state after all hangers yield.

3.4 Effect of steel plate thickness on local buckling of the rib

According to the above analysis, local buckling of the rib steel plate occurs after the ultimate

Table 2 Effect of the steel plate thickness changes Δt on the maximum load bearing capacity of the rib

Δt (mm)	10	5	0	-5	-10	-15
k	4.51	4.45	4.36	4.30	4.19	3.96

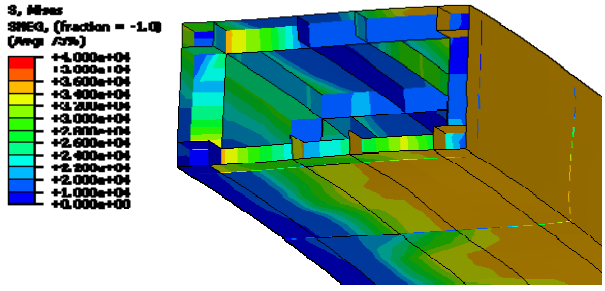

(a) Δt = 0 mm

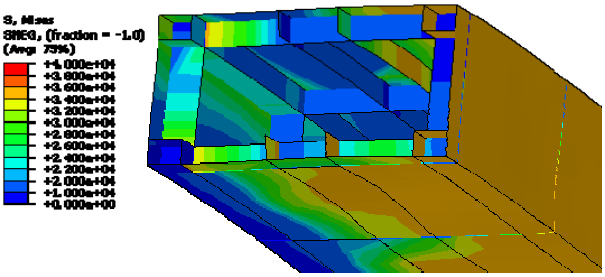

(b) Δt = -5 mm

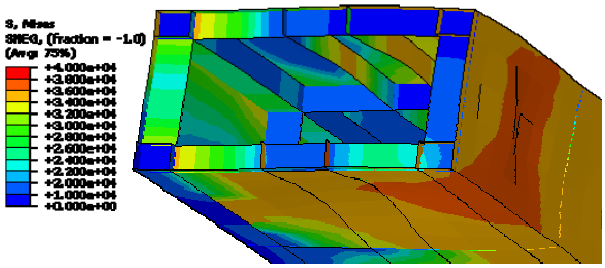

(c) Δt = -10 mm

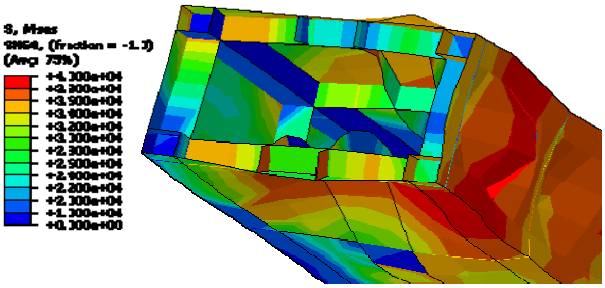

Δt = -15 mm

Fig. 12 Deformation and the plastic region distribution of the apex of the large arch (unit: 0.01 MPa)

load state. To investigate the influence of the thickness of the plate on the global stability, we analyzed the structure's bearing capacity for five different arch ribs with varying plate thickness as shown in Table 2. The analysis shows the structural strength improves as the plate thickness increases, but we didn't observe any significant decrease of the ultimate capacity caused by local buckling. Fig. 12 shows the distribution of the plastic region and the deformation at the crown of large arch rib at the limit state, and it demonstrates that significant reduce of the plate thickness would cause obvious local deformation before the structure reaches the limit load state, but the local deformation of steel plate has very minor impact on the ultimate capacity of the structure.

3.5 Effect of initial imperfections of the ribs

If we apply a small anti-symmetric deformation to the axis of a perfect arch rib, the failure mode of the arch will be limit point, rather than bifurcation (Pi and Trahair 1999, Pi *et al*. 2002), which is consistent with our calculation with consideration of geometric nonlinearity. Therefore, only the influence of residual stresses on the critical load of the bridge will be discussed in this section. Assume the residual stress of the arch rib is distributed in trapezoidal form across the cross section shown in Fig. 13, and the compressive residual stress is $0.4\sigma_y$. The load factor k - displacement d curves of the crown of the smaller arch rib under load case 1 are shown in Fig. 14. These curves are basically identical, suggesting the equilibrium paths are the same, and the residual stress has little impact on the stability of the bridge since the slenderness of the arch ribs is large enough (about 240).

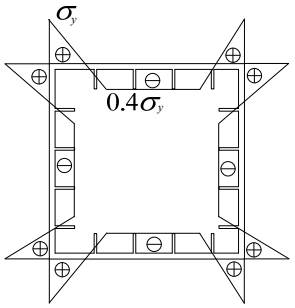

Fig. 13 Residual stress distribution at the cross section of arch rib

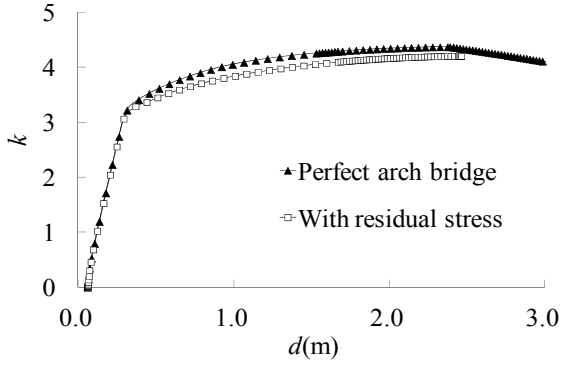

Fig. 14 Comparison of load factor-displacement curves on the structure

4. Validation of the accuracy for fiber model

Based on the previous analysis results, the deformation of the cross-section has little effect on the ultimate capacity of the structure. Therefore, an algorithm that does not consider the deformation of the cross-section may be feasible, which can greatly facilitate the design of the structure.

The fiber model is a beam element type model in which the deformation of cross-section will be ignored. It is usually used to check the stability of the steel arch bridge by designers. To validate the fiber model, we analyzed the structure using both fiber model and shell model. Fig. 15 shows the load-displacement curves at the crown of the larger rib under load case 1. The results illustrate that the load factor obtained from the fiber model and the shell model are similar, and the error in the engineering design is insignificant.

Fig. 16 shows the results when the rib plate thickness is reduced to 5 mm and 10 mm to verify the effect of the deformation of cross-section on the accuracy of fiber model. The difference between the two algorithms increases as the plate thickness increases, but the differences are insignificant for engineering design.

These results indicate that using fiber model to evaluate the strength of a special-shaped steel arch bridge is efficient and accurate.

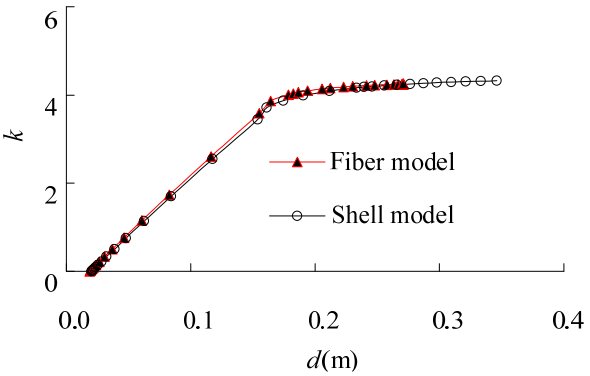

Fig. 15 Comparison of the load-displacement curves of the shell model and fiber model

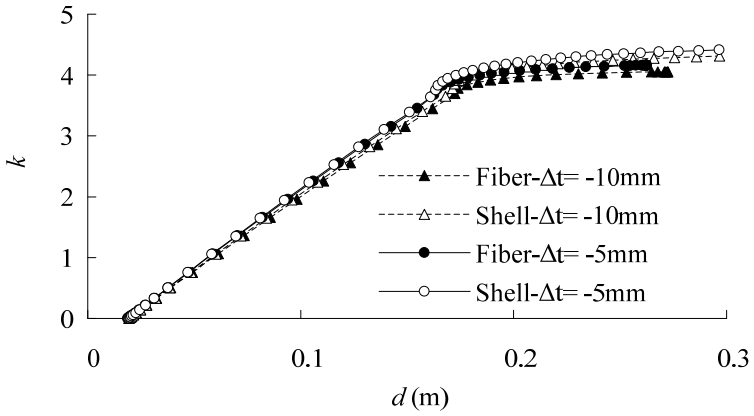

Fig. 16 Load-displacement curve of shell model and fiber model

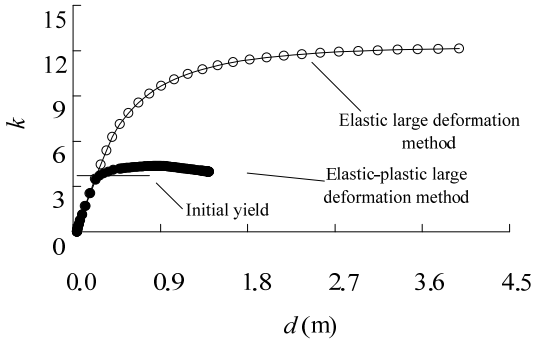

Fig. 17 Load-displacement curves obtained by elastic large deformation and elastic-plastic large deformation method

5. Analysis of elastic stability

To evaluate the influence of the yield strength of the material on the global stability of the structure, we performed stability analysis using elastic method with consideration of geometric nonlinearity. Fig. 17 only shows the vertical displacement at the top of the larger arch under load case 1 obtained by elastic and elasto-plastic methods since the results of the four load cases are similar to each other. After yielding of the arch rib in the structure, the results obtained by the elasto-plastic algorithm reaches the limit load state soon, while the LPF calculated by elastic algorithm continues to increase. The difference between the two algorithms could result from the decrease of modulus during the material hardening process. It demonstrates that plasticity of the arch rib has a significant impact on the bearing capacity of the structure. It is a simple and effective method to evaluate the stability strength of this kind of special-shaped steel arch based on yield strength of arch rib. Although this method is conservative, when consider the effects of the residual stress and initial imperfections of the structure, the actual capacity would not differ too much with what obtained from this simplified methodology.

6. Conclusions

Using three-dimensional elasto-plastic full-bridge model, this research performs in-depth studies on an asymmetric steel arch bridge with inclined ribs and hangers. The research results provide some profound understandings of the stability of steel arch bridges and the following conclusions may be drawn from this research.

- An arch bridge with asymmetric inclined rib has high stability strength because of the lateral constraint of its interior and exterior hangers. Improving the strength and stiffness of the hangers can enhance the ultimate capacity of the structure.
- Fully loaded case is the governing load case because the rib axial force is the largest in this case, which leads to the minimum structural load factor.
- An asymmetric steel arch bridge with inclined ribs and hangers starts to yield from the arch foot to 1/4 arch span. Structural damage is in the form of the lateral instability of the arch top. The load-displacement curve is similar to the material yield path. There is no significant decrease in capacity when instability occurs.

- Local buckling of the rib plate has little effect on the ultimate load factor of the bridge. Fiber model, which can not consider the local deformation of the rib, is a feasible and convenient method for structure design.
- Residual stress of the arch ribs has little impact on the global stability of the bridge, load-displacement curves of the arch structure with and without residual stress are basically identical.
- The yield strength of the arch rib has an significant effect on the structural bearing capacity since the structure can only bearing a little more after the initial yielding state of the rib, thus the initial yielding state of the arch rib can be treated approximately as the ultimate state of the structure from a conservative point of view.

References

Austin, W.J. and Ross, T.J. (1976), "Elastic buckling of arches under symmetrical loading", *J. Struct. Div*., *ASCE*, **102**(5), 1085-1095.

Dadeppo, D.A. and Schmidt, R. (1969), "Nonlinear analysis of buckling and post buckling behavior of circular arches", *J. Appl. Math. Phys.* **20**(6), 847-857.

Cai, J.G. and Feng, J. (2010), "Buckling of parabolic shallow arches when support stiffens under compression", *Mech. Res. Commun.,* **37**(5), 467-471.

Cai, J.G., Feng, J., Xu, Y.X. and Zhang, J. (2012), "Effects of temperature variations on the in-plane stability of steel arch bridges", *J. Bridge Eng., ASCE*, **17**(2), 232-240.

Cheng, J. and Li, Q.S. (2009), "Reliability analysis of a long span steel arch bridge against wind-induced stability failure during construction", *J. Constr. Steel Res.*, **65**(3), 552-558.

Cheng, J., Jiang, J.J., Xiao, R.C. and Xiang, H.F. (2003), "Ultimate load carrying capacity of the Lu Pu steel arch bridge under static wind loads", *Comput. Struct.,* **81**(2), 61-73.

Kim, S., Choi, S. and Ma, S. (2003), "Performance based design of steel arch bridges using practical inelastic nonlinear analysis", *J. Constr. Steel Res.*, **59**(1), 91-108.

Moon, J., Yoon, K.Y., Lee, T.H. and Lee, H.E. (2009), "In-plane strength and design of parabolic arches", *Eng. Struct.*, **31**(2), 444-454.

Pi, Y.L. and Bradford, M.A. (2010a), "Nonlinear thermoelastic buckling of pin-ended shallow arches under temperature gradient", *J. Eng. Mech., ASCE*, **136**(8), 960-968.

Pi, Y.L. and Bradford, M.A. (2010b), "In-plane thermoelastic behavior and buckling of pin-ended and fixed circular arches", *Eng. Struct.*, **32**(1), 250-260.

Pi, Y.L. and Bradford, M.A. (2010c), "Nonlinear in-plane elastic buckling of shallow circular arches under uniform radial and thermal loading", *Int. J. Mech. Sci.*, **52**(1), 75-88.

Pi, Y.L. and Trahair, N.S. (1999), "In-plane buckling and design of steel arches", *J. Struct. Eng.*, **125**(11), 1291-1298.

Pi, Y.L., Bradford, M.A. and Uy, B. (2002), "In-plane stability of arches", *J. Solids Struct.*, **39**(1), 105-125.

Romeijn, A. and Bouras, C. (2008), "Investigation of the arch in-plane buckling behavior in arch bridges", *J. Constr. Steel Res.*, **64**(12), 1349-1356.

Wei, J.G., Wu, Q.X., Chen, B.C. and Wang, T. (2009), "Equivalent beam-column method to estimate in-plane critical loads of parabolic fixed steel arches", *J. Bridge Eng.*, *ASCE*, **14**(5), 346-354.

Xie, X., Li, H. and Huang, J.Y. (2004), "Study on in-plane stability of long-span two-hinged arch bridges", *China Civil Eng. J.*, **37**(8), 43-49. [In Chinese]

CC